

Monte Carlo simulations of μCF processes kinetics in deuterium gas

Andrzej Adamczak

*Institute of Nuclear Physics, Polish Academy of Sciences, Kraków, Poland,
and Rzeszów Technical University, Rzeszów, Poland,*

Mark P. Faifman

Russian Research Center “Kurchatov Institute”, Moscow, Russia.

Abstract

The muon-catalyzed-fusion processes in D_2 gas for various temperatures and densities have been studied by means of Monte Carlo simulations. In particular, the role of the resonant and nonresonant $dd\mu$ formation and differences between the neutron time spectra from the ortho- D_2 and para- D_2 targets at low temperatures have been investigated.

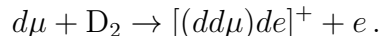
The negative muons which slow down in a D_2 target form the $d\mu$ muonic hydrogen atoms in the highly excited Rydberg states. Then, such atoms undergoing the various cascade processes [1] deexcite to the ground 1S state and participate in numerous processes accompanying μCF (muon-catalyzed-fusion) phenomenon [2]. The ground-state 1S atoms can gain high kinetic energies up to ~ 1000 eV, as a result of several accelerating collision processes during the atomic cascade (see, e.g., Refs. [3, 4, 5, 6]). However, a fraction of the 1S muonic atoms is thermalized after the cascade.

The aim of this work is to study the role of “hot” $d\mu$ atoms, supplied by the cascade, and the competition between the energy-dependent processes (muonic atom scattering and muonic molecule formation) of μCF cycle in a pure deuterium D_2 gas.

The D_2 targets simulated in our Monte Carlo calculations correspond to the D_2 targets which are to be used at JINR in the upcoming experiment [7] on the radiative capture reaction $d+d \rightarrow {}^4\text{He} + \gamma$ in the $dd\mu$ muonic molecule. The deceleration, thermalization and diffusion of $d\mu$'s in D_2 perfect gas is described using the differential scattering cross sections. At collision energies ε greater than about 1 eV, the doubled cross section for $d\mu$ scattering from the bare deuterium nuclei are employed [8, 9]. At lower energies, where molecular binding and electron-screening effects are significant, the differential cross sections for $d\mu$ scattering from isolated D_2 molecules are used [10]. The total “molecular” and “nuclear” cross sections are smoothly sewed together, which was presented in Ref. [11]. The cross sections used take into account the spin-flip of $d\mu$ atom and the rotational-vibrational excitations of the target molecules. For the considered temperatures $T = 40\text{--}300$ K, the D_2 molecules are in the ground vibrational state $\nu = 1$. The population of the total spin states $F = 1/2$ and $3/2$ after the cascade is assumed to be statistical.

The $d\mu$ atoms can form the muonic molecules $dd\mu$ in collision with the D_2 molecules. Such a process can have both the nonresonant or resonant character [2]. The latter is possible due to the presence of the loosely-bound state rotational-vibrational state $J =$

$v = 1$ of $dd\mu$ [12]. The energy excess in nonresonant $dd\mu$ formation is taken away by the electron [13]



The rate of this reaction is practically independent of the $d\mu$ atom spin. At $\varepsilon \lesssim 100$ eV, only the s and p waves give significant contributions to the formation rate. In Fig. 1, the calculated rate of nonresonant $dd\mu$ formation in $d\mu$ collision with a free D_2 molecule is plotted versus $d\mu$ energy [13]. The formation rates in this paper are given for the target density $\phi = 1$ in the liquid hydrogen density units (LHD). The nonresonant $dd\mu$ formation

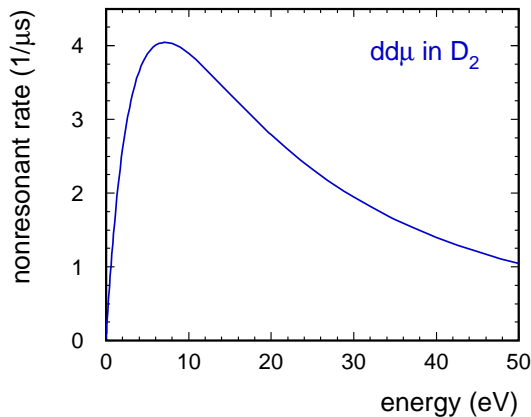


Figure 1: The rate of nonresonant $dd\mu$ formation in $d\mu$ scattering from D_2 gas versus $d\mu$ energy.

rate is significant ($\sim 1 \mu s^{-1}$) even at a few tens eV, has maximum at $\varepsilon \approx 7$ eV, and falls rapidly when $\varepsilon \rightarrow 0$.

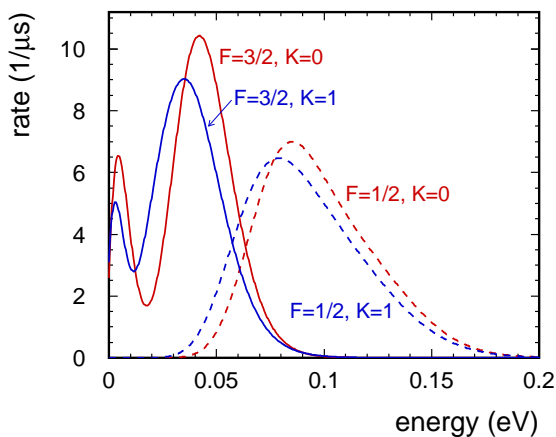
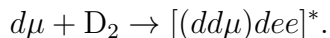


Figure 2: The effective rate of resonant $dd\mu$ formation in $d\mu$ scattering from 40-K ortho- D_2 ($K = 0$) and para- D_2 ($K = 1$) gas versus $d\mu$ energy. The solid lines correspond to the upper spin state $F = 3/2$ of $d\mu$, the dashed lines describe the $F = 1/2$ state.

In the resonant $dd\mu$ formation, the energy excess is transferred to rotational-vibrational excitations of the muonic-molecular complex



The resonant rate strongly depends on the $d\mu$ energy and its total spin state F . In Fig. 2, the effective resonant $dd\mu$ rate (with the back decay of $dd\mu$ included) for the perfect D_2 -gas target at 40 K, calculated according to the method presented in Ref. [14], is shown for the states $F = 3/2$ and $1/2$. Comparing Figs. 1 and 2, one can see that the resonant formation dominates at lowest energies ($\varepsilon \lesssim 0.1$ eV). The resonant rates calculated for the rotational states $K = 0$ and 1 of the target D_2 molecule display significant differences. As a result, the time spectra of $d-d$ fusion products should expect appreciable ortho-para effect at low temperatures.

The Monte Carlo simulations for the 40-K D_2 target have been performed using the nonresonant $dd\mu$ formation rates shown in Fig. 1. The resonant $dd\mu$ formation has been described using the absolute resonant formation rates and the back-decay rates. Since the mean free path of $d\mu$'s is much smaller than the dimensions of the JINR target (the volume of 180 cm^3), the simulations have been carried out for the infinite D_2 target. The nitrogen contamination of 10^{-6} have been taken into account. The reliable theoretical distribution of $d\mu$ energy after the cascade process is not calculated yet. Therefore, following Ref. [3], the initial $d\mu$ energy is assumed to be a sum of the two Maxwell distributions. The first Maxwell component corresponds to the nonthermalized $d\mu$'s and the second one describes the thermalized atoms. A relative population of these two groups of $d\mu$'s is used as a free parameter in our simulations.

In Figs. 3–6 are shown some results of our calculations for the 40-K D_2 gas. The mean energy ε_{avg} of $d\mu$'s in the both spin states is shown in Fig. 3 for short times. Only the

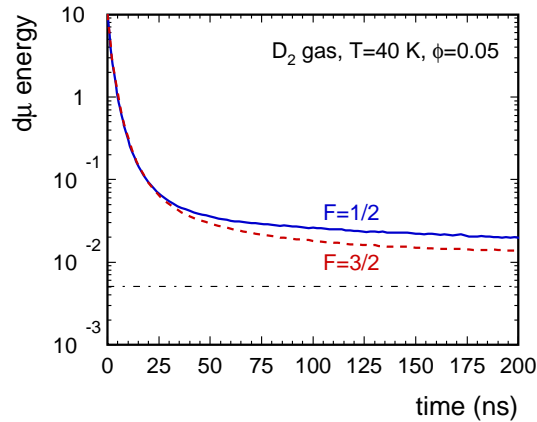
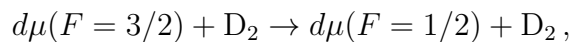


Figure 3: Mean kinetic energy of $d\mu(F = 1/2)$ and $d\mu(F = 3/2)$ atoms in D_2 gas ($T = 40$ K, density $\phi = 0.05$) versus time. The initial $d\mu$ energy distribution has the Maxwellian form with the mean energy of 10 eV.

nonthermalized Maxwell component with $\varepsilon_{\text{avg}} = 10$ eV has been considered, in order to study the $d\mu$ deceleration from high energies. One sees that slowing down to 0.05 eV is very fast — it takes about 25 ns. Then, this process is much slower since $d\mu$'s can gain appreciable energy due to the thermal motion of the target D_2 molecules. At this stage of thermalization a difference between the mean energies in the states $F = 1/2$ and $3/2$ is apparent. This is caused by the downwards spin-flip reaction



in which the energy $\Delta E_{\text{hfs}} = 0.0495$ eV (in the $d\mu + d$ center of mass) is released. The dash-dotted line shows the thermal energy of 0.005 eV corresponding to $T = 40$ K. The

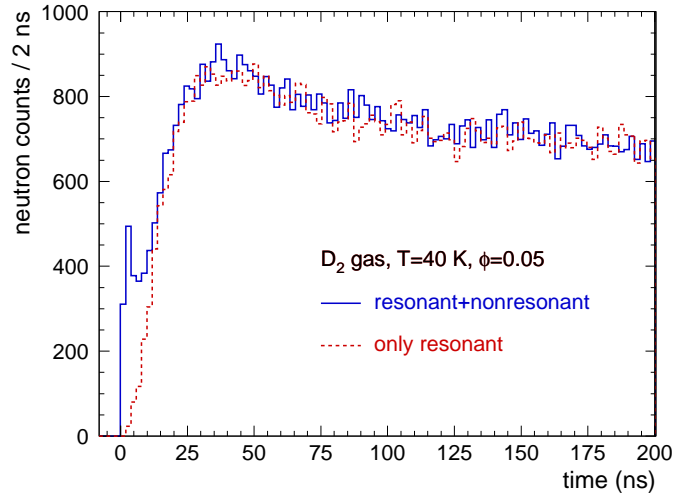


Figure 4: Spectrum of neutrons from d - d fusion in D_2 gas ($T = 40$ K, density $\phi = 0.05$) for short times. The contributions from all $dd\mu$ formation processes and from resonant process are shown separately.

time spectra of neutrons from muon-catalyzed d - d fusion for the same initial conditions are shown in Fig. 4. The solid line represents the time spectrum with both the resonant and nonresonant $dd\mu$ formation processes taken into account. The dashed line has been obtained assuming only the presence of the resonant formation. At short times ($\lesssim 20$ ns) the fusion is mainly due to the nonresonant $dd\mu$ formation since most $d\mu$'s are not slowed down to the energies corresponding to the resonance peaks. This phenomenon is more pronounced at lower target densities [15].

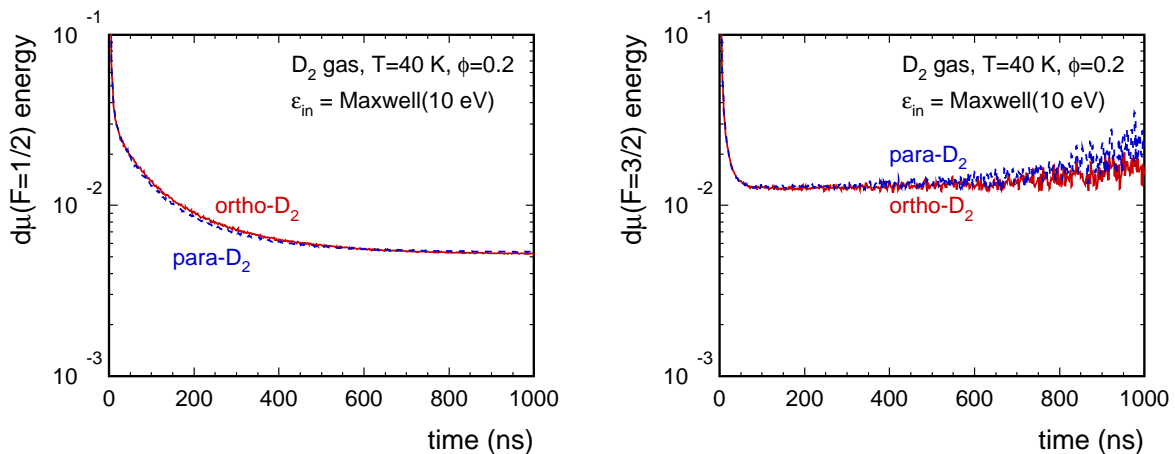


Figure 5: Mean kinetic energy of $d\mu(F = 1/2)$ and $d\mu(F = 3/2)$ atoms in ortho- D_2 and para- D_2 gas ($T = 40$ K, density $\phi = 0.2$) versus time. The initial $d\mu$ energy distribution has the Maxwellian form with the mean energy of 10 eV.

When the temperature of a 300-K D_2 gas is lowered, the even rotational states deexcite to $K = 0$ and the odd rotational states fall to $K = 1$, because of the symmetry of the

D₂ wave function. As a result, the cooled deuterium target forms the statistical mixture (2:1) of the ortho-D₂ and para-D₂ molecules [16]. The deceleration of $d\mu(F = 3/2)$ and $d\mu(F = 1/2)$ atoms in ortho-D₂ and para-D₂ targets at $T = 40$ K and $\phi = 0.2$ is illustrated in Fig. 5. The ground-state $d\mu(F = 1/2)$ atoms are fully thermalized after about 1000 ns. On the other hand, the mean energy of the $d\mu(F = 3/2)$ atoms never reaches the thermal value. The initial population of these excited atoms disappears after a few hundreds ns. For larger times, one sees only a very small amount of the $d\mu(F = 3/2)$ atoms that are created via the back decay of the muonic-molecular complex $[(dd\mu)dee]$. In this process, they gain appreciable kinetic energy.

Ortho-para effects in μ CF in solid, liquid, and cold-gas D₂ targets with different concentrations of ortho-D₂ molecules have been experimentally studied [17, 18]. The measured ortho-para effects in solid deuterium targets (stronger resonant $dd\mu$ formation in para-rich D₂) are opposite to those predicted by theory [19], which requires further experimental and theoretical investigations. On the other hand, theory and experiment give the same sign of the ortho-para effect in the case of cold D₂ gases.

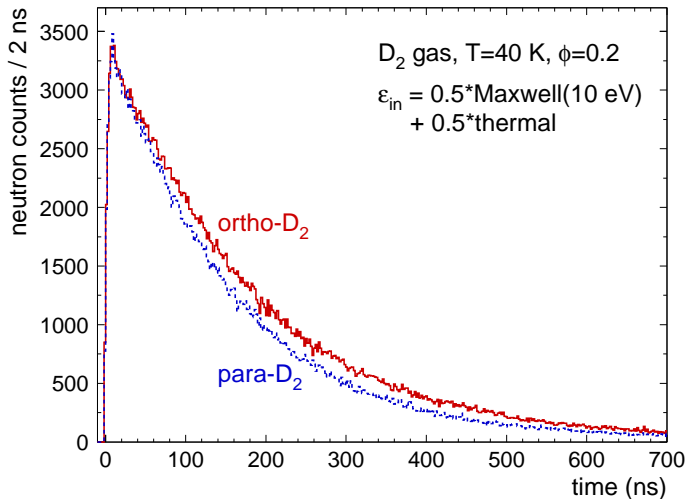


Figure 6: Time spectrum of neutrons from d - d fusion in ortho-D₂ and para-D₂ gas at $T = 40$ K and density $\phi = 0.2$.

The calculated fusion-neutron time spectra for ortho-D₂ and para-D₂ gas at $T = 40$ K and $\phi = 0.2$ are shown in Fig. 6. The two-Maxwell distribution [3] of the initial $d\mu$ energy has been assumed. After short time, the number of neutrons in ortho-D₂ case is significantly greater than in the para-D₂ target. This difference disappears at much larger times. Such a bump in the ortho-rich D₂ target at similar conditions has been experimentally observed [18]. Thus, the theory agrees with the experimental findings, at least qualitatively.

In Figs. 7–10 are presented our theoretical results for the D₂ perfect-gas target at 300 K. The effective resonant formation rates for $F = 1/2$ and $3/2$ are plotted in Fig. 7. These functions are more flat than those in Fig. 2 since the thermal distribution of D₂ energies is much broader at 300 K and more initial rotational states are significantly populated at this temperature. Figure 8 shows the Monte Carlo time evolution of the population of the $d\mu(F = 3/2)$ atoms at 300 K and $\phi = 0.5$. The initial statistical value of the upper-spin population is equal to $2/3$. After about 200 ns, the thermal equilibrium between the lower

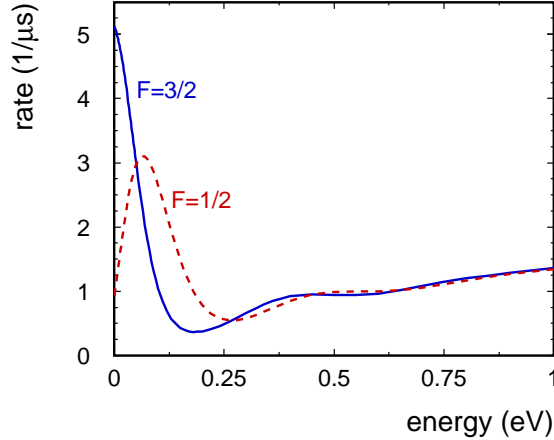


Figure 7: The rate of resonant $dd\mu$ formation in $d\mu$ scattering from 300-K D_2 gas versus $d\mu$ energy. The solid lines correspond to the upper spin state $F = 3/2$ of $d\mu$, the dashed lines describe the $F = 1/2$ state.

and upper spin states is reached. The theoretical downwards spin-flip rate has been scaled by the constant factor of 0.6, determined by comparison with the experimental results [20]. The thermalization of $d\mu$ atoms at such a density is very fast — it takes only a few ns.

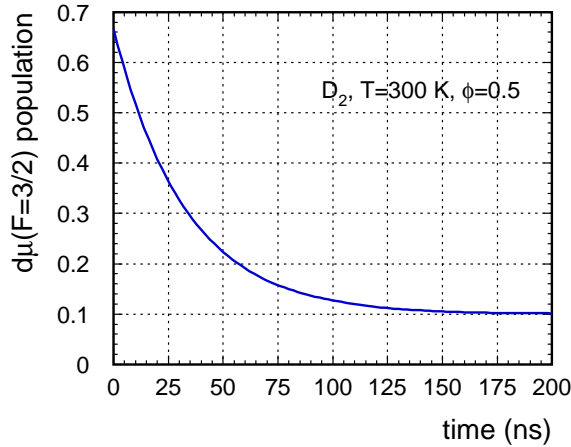


Figure 8: Time evolution of the spin state $F = 3/2$ fusion in D_2 gas ($T = 300$ K, density $\phi = 0.5$).

Therefore, the initial $d\mu$ -energy distribution does not affect the fusion-product spectra at significantly larger times.

The calculated neutron time spectrum for this D_2 target is plotted in Fig. 9, for very large time interval. Apart from the prompt peak, the spectrum can be well described by the steady-state kinetics. The Monte Carlo spectra of fusion neutrons and electrons from muon decays are shown for short times in Fig. 10. The electron spectrum is flat since the muon decay does not depend on the $d\mu$ atom energy.

In conclusion, the theoretical results of Monte Carlo simulations of the μ CF cycle processes in gaseous D_2 targets, corresponding to the JINR target conditions, have been obtained. The theoretical resonant and nonresonant $dd\mu$ formation rates and the differential

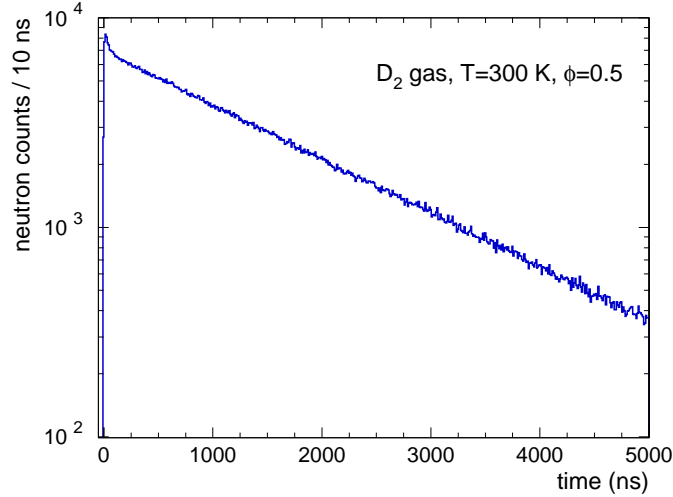


Figure 9: Time spectrum of neutrons from d - d fusion in D_2 gas at $T = 300$ K and at density $\phi = 0.5$.

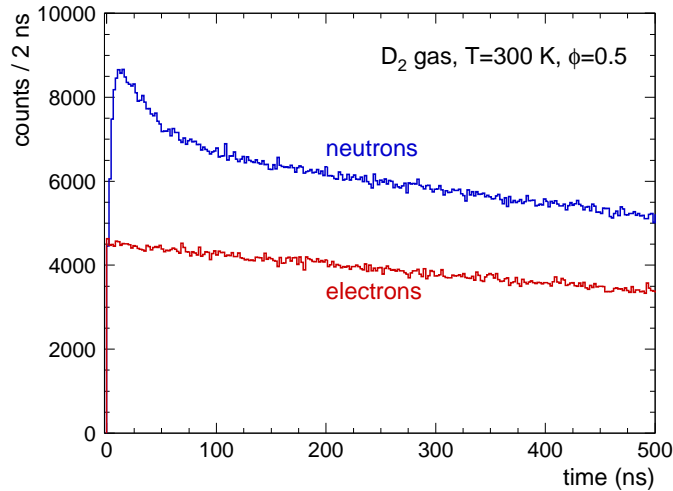


Figure 10: Time spectra of fusion neutrons and of electrons from muon decay in D_2 gas at $T = 300$ K and at density $\phi = 0.5$.

cross sections for $d\mu$ scattering from D_2 molecules established the input for our calculations. In particular, the thermalization of $d\mu$ atoms for various targets and the role of nonresonant $dd\mu$ formation in short-time neutron spectra have been investigated. The nonresonant formation can be directly observed at very short times in low-temperature targets at densities $\phi \lesssim 0.05$. Also, the $d\mu$ -thermalization time is important at relatively low target densities. The calculated neutron time spectra for ortho- D_2 and para- D_2 at 40 K and $\phi = 0.2$ display the enhanced neutron emission in the ortho-rich targets at intermediate times, which agrees qualitatively with the recent experimental data. The simulation for the high density ($\phi = 0.5$) D_2 target at 300 K shows that the neutron time spectrum can be well described by the steady-state kinetics, apart from very short times.

This work was supported by the INTAS grant Nr 05-1000008-7953.

References

- [1] M. Leon, and H. A. Bethe, Phys. Rev. **127**, 636 (1962).
- [2] L. I. Men'shikov, L. I. Ponomarev, T. A. Strizh and M. P. Faifman, Zh. Eksp. Teor. Fiz. **92**, 1173 (1987) [Sov. Phys. JETP **65**, 656 (1987)].
- [3] D. J. Abbott et al., Phys. Rev. A **55**, 214 (1997).
- [4] R. Pohl et al., Hyperfine Interact. **138**, 35 (2001).
- [5] M. P. Faifman and L. I. Menshikov, Hyperfine Interact. **138**, 61 (2001).
- [6] T. S. Jensen, and V. E. Markushin, Eur. Phys. J. D **21**, 271 (2002).
- [7] D. L. Demin et al., INTAS project Nr 05-1000008-7953, 2005.
- [8] M. Bubak and M. P. Faifman, report JINR E4-87-464, Dubna (1987).
- [9] L. Bracci et al., Muon Catal. Fusion **4**, 247 (1989).
- [10] A. Adamczak, Phys. Rev. A **74**, 042718 (2006).
- [11] A. Adamczak et al., At. Data Nucl. Data Tables **62**, 255 (1996).
- [12] E. A. Vesman, Pis'ma Zh. Eksp. Teor. Fiz. **5**, 113 (1967) [JETP Letters **5**, 91 (1967)].
- [13] M. P. Faifman, Muon Catal. Fusion **4**, 341 (1989).
- [14] M. P. Faifman, L. I. Menshikov and T. A. Strizh, Muon Catal. Fusion **4**, 1 (1989).
- [15] D. V. Balin et al., report PNPI-2729, Gatchina, 2007.
- [16] P. C. Souers, *Hydrogen Properties for Fusion Energy*, University of California Press, Berkeley, 1986.
- [17] A. Toyoda et al., Phys. Rev. Lett. **90**, 243401 (2003).
- [18] H. Imao et al., Phys. Lett. B **632**, 192 (2006) and talk at the International Conference on Muon Catalyzed Fusion and Related Topics μ CF-07, Dubna, 18–21 June, 2007.
- [19] A. Adamczak and M. P. Faifman, Phys. Rev. A **64**, 052705 (2001).
- [20] N. I. Voropaev et al., Hyperfine Interact. **138**, 331 (2001).